ACS APPLIED MATERIALS & INTERFACES

Research Article

www.acsami.org

Surface-Dependent Localized Surface Plasmon Resonances in CuS Nanodisks

Tiaoxing Wei,[†] Yufeng Liu,[‡] Wenjing Dong,[†] Yun Zhang,[†] Chanyan Huang,[†] Yan Sun,[†] Xin Chen,*[,†] and Ning Dai*[,†]

[†]National Laboratory for Infrared Physics, Shanghai Institute of Technical Physics, Chinese Academy of Sciences, Shanghai 200083, China

[‡]CAS Key Laboratory of Materials for Energy Conversion and State Key Laboratory of High Performance Ceramics and Superfine Nanostructure, Shanghai Institute of Ceramics, Chinese Academy of Sciences, Shanghai 200050, China

Supporting Information

ABSTRACT: We demonstrated revertible shifts of surface-dependent localized surface plasmon resonances (LSPRs) in CuS nanodisks. Oleylamine (OYA) served as a solvent and surface ligand covering on CuS nanodisks during the thermolysis of single-source precursor copper ethylxanthate ($Cu(ex)_2$). When OYA ligand was unloaded and reloaded on the surface of CuS nanodisks, the wavelength of LSPRs blue-shifted due to more oxygen exposure and then reverted through surface repassivation. The surface-dependent shift of LSPRs was dominated by the concentration of free holes in CuS nanodisks, which was modulated by the coverage and exchange of surface ligands, and the oxygen exposure dose and time. The semiconductor nanocrystals with tunable LSPRs have great potential in advanced plasmonics.

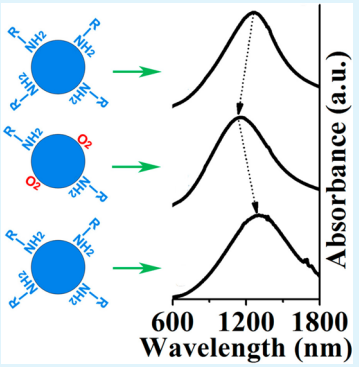

KEYWORDS: *copper sulfide, nanocrystals, absorption spectra, localized surface plasmon resonance, surface ligand, free carrier*

1. INTRODUCTION

Localized surface plasmon resonances (LSPRs), coupling between optical field and collective oscillation of free carriers in nanostructures, have been implicated in the fundamental principle behind biosensors, surface enhanced Raman spectroscopy, near-field optics, and plasmonic metamaterials.[1−3] In general, LSPRs have been widely modeled and achieved in noble metal (e.g., gold and silver) nanostructures.[4] Nevertheless, doped-semiconductor nanocrystals recently exhibited great potential as building blocks in plasmonic nanomaterials for LSPRs.[5−9] Doped semiconductors, in comparison with metals, have a key advantage of tunable free carrier concentrations, which allows for tuning the dielectric properties according to the Drude model.[6] This advantage benefits the engineering, controlling, or switching of LSPRs at a specified wavelength.[5,7] Copper chalcogenides, $Cu_{2-x}S$,[6] $Cu_{2-x}Se$,[10] and $Cu_{2-x}Te$,[11] nanocrystals in particular, have attracted increasing attention due to tunable LSPRs in the near-infrared region. Meanwhile, copper monosulfide (CuS, covellite) nanocrystals have been under wide discussion on the origin of the remarkable near-infrared absorption band.[12−15] It has been demonstrated by Hall measurements that CuS has metallic hole conduction, and one-third of holes may exist in one chemical formula unit of CuS.[16] This high concentration of p-type free carriers benefits LSPRs in CuS nanostructures according to the Drude model.[6]

Besides, LSPRs in plasmonic $Cu_{2-x}S$ nanocrystals have been demonstrated to be tuned by the media dielectric constant, shape, size, and components.[6,10,17−19] The resonant wavelength of LSPRs blue-shifts from $Cu_{1.97}S$ to $Cu_{1.8}S$ to CuS as the self-doping induced free carrier concentration decreases.[20] Furthermore, oxidizing and reducing agents have been exploited to tune LSPRs in copper chalcogenide nanocrystals.[6,10,11] The oxidation of stoichiometric Cu_2S and Cu_2Se nanocrystals into non-stoichiometric $Cu_{2-x}S$ and $Cu_{2-x}Se$ nanocrystals can accelerate the generation of LSPRs. All of these LSPRs are based on the tunable hole concentration induced by the copper vacancies in copper chalcogenide nanocrystals. Here, we demonstrate the revertible shifts of LSPRs by unloading and reloading surface ligand on CuS nanodisks obtained by the thermolysis of $Cu(ex)_2$. Oxygen exposure and repassivation on the surface of CuS nanocrystals are responsible for the revertible shifts, and the effects of ligand coverage, oxygen exposure dose, and time are also studied. The surface-dependent LSPRs are modulated by the electron-withdrawing ability of surface adsorbed species which can adjust the free hole density in CuS nanodisks.

Received: May 8, 2013
Accepted: October 18, 2013
Published: October 18, 2013

2. EXPERIMENTAL SECTION

2.1. Preparation of CuS Nanocrystals. All chemicals were used as received. $Cu(ex)_2$ was obtained according to the following processes. A 10 mmol portion of copper(II) chloride ($CuCl_2$, Aldrich, 99.999%) and 20 mmol of postassium (I) ethylxanthate ($C_3H_5OS_2K$, Aldrich, 96%) were dissolved in 40 mL of distilled water, respectively. When we added the aqueous solution of $CuCl_2$ into the $C_3H_5OS_2K$ aqueous solution, the yellow precipitates formed simultaneously. Then, the yellow precipitates were filtered and washed three times with distilled water. Finally, the product was dried in a vacuum, and used as the precursor for CuS nanocrystals. During a typical synthesis of CuS nanocrystals, 8 mL of oleylamine (OYA, approximate C18 content 80−90%, Acros) was added in a 50 mL three-neck flask and heated to 130 °C to degas for 30 min in an argon atmosphere. In a glovebox (H_2O < 1 ppm, O_2 < 1 ppm), 0.2 mmol of $Cu(ex)_2$ was dissolved in 4 mL of OYA for obtaining the precursor solution. The precursor solution containing $Cu(ex)_2$ and OYA was injected quickly into the hot OYA in a three-neck flask at 230 °C. Once the precursor was injected, the reaction temperature dropped down to 200 °C immediately. Subsequently, the reaction mixture was taken out by a syringe after 30 s, and injected into 20 mL of OYA to quench the reaction. Finally, the resulting nanocrystals were collected by the following surface-treatment cycle inside the glovebox: (I) 1 mL of reaction mixture was flocculated by adding 2 mL of acetone; (II) a centrifugation process was performed at 10000 rpm to collect the CuS nanocrystals; (III) 1 mL of tetrachloroethylene (TCE) was used to disperse the centrifuged CuS nanocrystals. No size selection was performed during the surface-treatment cycle. The surface-treatment cycle can be repeated to remove more organic ligands off the surface of CuS nanocrystals.

2.2. Oxygen Exposure and Repassivation. A 1 mL portion of TCE containing the CuS nanodisks was placed in a 5 mL centrifuge tube, and taken out from the glovebox. Then, it was exposed in air for 30 min, and stored under ambient conditions after the centrifuge tube was reclosed with a cap and violently shaken. For a repassivation process, 0.5 mL of OYA was added to 1 mL of TCE containing the CuS nanodisks which had been stored under ambient conditions for 48 h after being exposed as mentioned above. The nanodisks were recollected by adding 2.5 mL of acetone followed by a centrifugation process, and then, they were redispersed in 1 mL of TCE.

2.3. Surface Ligand Exchange. In a glovebox, 0.5 mL of TCE containing the CuS nanodisks was mixed with 0.5 mL of oleic acid (OA, Aldrich, 99%) after one surface-treatment cycle. They were placed in a centrifuge tube under ultrasonic agitation for 1 min as mentioned above. Subsequently, the CuS nanodisks were collected by adding 2 mL of acetone followed by centrifugation processes. Then, the CuS nanodisks were dispersed in TCE again for making measurements of absorption spectra. When we used 1-dodecanethiol (DDT, Aldrich, >98%) to exchange the surface ligand OYA, all processes were the same as those in the OA case.

2.4. Characterization. Transmission electron microscopy (TEM) and high resolution transmission electron microscopy (HRTEM) images were taken on a JEM-2100F instrument equipped with a Gatan 832 CCD at an acceleration voltage of 200 kV. TEM samples were prepared by dropping dispersed CuS nanocrystals onto carbon-coated copper grids. The X-ray diffraction (XRD) pattern was tested on a Bruker D8 Discover X-ray diffractometer equipped with Cu Kα radiation (λ = 1.54056 Å). X-ray photoelectron spectroscopy (XPS) was acquired using a Krotos AXIS Ultra DLD X-ray photoelectron spectrometer. UV−vis−NIR absorbance spectra were collected by a Lambda 950 instrument. Fourier transform infrared spectroscopy (FTIR) was measured by a Vertex 70 (Bruker). Thermogravimetric analysis (TGA) was measured using NETZSCH STA 449C thermal analysis instruments with a ramp rate of 10 °C/min under nitrogen.

3. RESULTS AND DISCUSSION

Figure 1a shows CuS nanocrystals obtained by thermolysis of $Cu(ex)_2$ in hot OYA. Thermolysis of single-source precursor $Cu(ex)_2$ provides a convenient phosphine-free method without separated Cu and S precursors for the synthesis of CuS nanocrystals. As we previously demonstrated, metal ethylxanthates are facile, inexpensive, and stable precursors for the synthesis of chalcogenide nanocrystals.[21] The decomposition of $Cu(ex)_2$ started at 140 °C and finished at 205 °C when ~61% of the initial weight lost, as revealed by TGA curve (Figure S1, Supporting Information). Therefore, the injection temperature was set at 230 °C during the preparation of CuS nanocrystals. When the $Cu(ex)_2$ solution was injected into the hot OYA, the instant decomposition of $Cu(ex)_2$ benefited homogeneous nucleation. Subsequent gentle heating promoted controllable growth and annealing of nanocrystals.

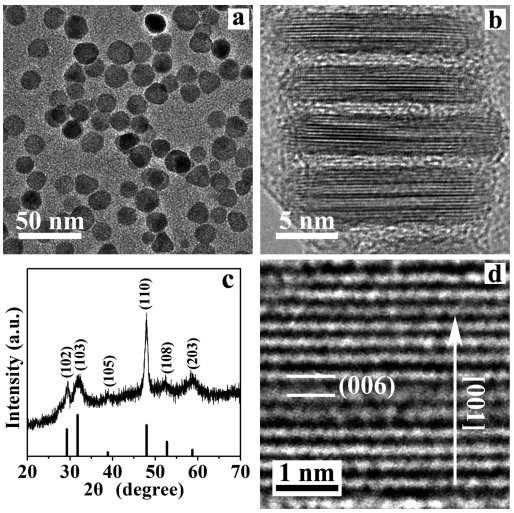

Figure 1. TEM images of flatwise (a) and upright (b) CuS nanodisks. XRD pattern (c) reveals as synthesized nanodisks to be covellite CuS. HRTEM (d) of upright CuS nanodisks. CuS nanocrystals obtained by quick injection of $Cu(ex)_2$ (0.2 mmol in 4 mL of OYA) into hot OYA.

Some nanocrystals assemble together, as shown in Figure 1b, which demonstrates the nanocrystals are disk-like in contrast to Figure 1a. The lateral size of nanodisks is ~15.2 nm with a thickness of ~3.8 nm, which is based on the statistic evaluation of 100 nanodisks in TEM images of the assembled structures. The XRD pattern in Figure 1c reveals the nanodiskes to be stoichiometric covellite (CuS) by comparing the diffraction patterns with the JPCD card (06-0464). A further HRTEM (Figure 1d) image of the individual nanodisk in the assembled structure indicates that the thickness of nanodisks is in the [001] direction and the lateral plane is parallel to the (006) crystallographic plane. Thus, we note that these CuS nanodisks can self-assemble with their lateral planes facing each other, and arrange along the [001] direction. The axial interdisk space is ~0.8 nm, and less than the chain length (~2 nm) of the OYA molecule, implying that the assembly may be drove by dipolar−dipolar interaction among CuS nanodisks.[22,23]

Figure 2a displays the high-resolution XPS spectrum of Cu 2p at 932.42 and 952.22 eV for Cu 2p3/2 and Cu 2p1/2, respectively. The slight asymmetry in the peak shape of Cu 2p and a small satellite between these two peaks reveal the presence of Cu(II).[12] The binding energies of S 2p3/2 at 162 eV and S 2p1/2 at 163 eV are shown in Figure 2b. The molar ratio of Cu/S is 1.002 obtained by analyzing the integrated areas of Cu and S in the XPS spectra. As we know, the copper sulfide comes from a family of binary compounds of copper and sulfur, including five stable phases at room temperature, i.e., covellite (CuS), anilite ($Cu_{1.75}S$), digenite ($Cu_{1.8}S$), djurleite

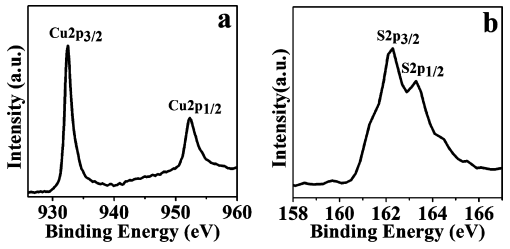

Figure 2. XPS spectra of Cu (a) and S (b) in CuS nanodisks.

($Cu_{1.94}S$), and chalcocite (Cu_2S).[24] These XPS measurements indicate that the copper sulfide nanodisks are the covellite (CuS) phase,[25] which is in good agreement with that confirmed by XRD.

UV–vis–NIR spectroscopy (Figure 3a) shows an obvious near-infrared absorption band of CuS nanodisks dispersed in

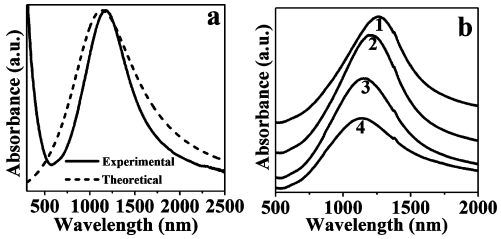

Figure 3. (a) Comparison of experimental and theoretical UV–vis–NIR absorption spectra of CuS nanodisks dispersed in TCE. (b) Blue-shift of LSPRs (curves 1–4) with increasing surface-treatment cycles with identical oxygen-exposure time.

TCE. There is a band edge absorption offset wavelength around 570 nm matching the band gap energy of CuS.[26] As demonstrated in non-stoichiometric copper sulfide nanocrystals for LSPRs,[6,17,18,20] the near-infrared absorption is ascribed to LSPRs which result from optical coupling with carrier collective oscillation in CuS nanodisks. As mentioned above, CuS has been demonstrated to possess larger p-type conductivity than other phases of copper sulfides due to its crystal structure and chemical valence state.[16,26–30] According to the Drude model, the LSPR frequency (ω_{sp}) is obtained as follows:[8,17]

$$\omega_{sp} = \sqrt{\frac{\omega_p^2}{1 + \frac{1 - L_j}{L_j}\varepsilon_m} - \gamma^2} \quad (1)$$

where L_j is a shape-dependent geometrical factor with j = 1, 2, or 3 presenting three axes of the nanoparticle, ε_m is the dielectric constant of the surrounding medium, and γ is the collision frequency term. ω_p is the bulk plasma frequency with expression

$$\omega_p = \sqrt{\frac{N_h e^2}{\varepsilon_0 m_h}} \quad (2)$$

where N_h is the free hole density, e is the electron charge, ε_0 is the free space permittivity, and m_h is the hole effective mass. All of these are based on the resonance condition for dipolar polarizability in quasi-electrostatic approximation where the size of nanoparticles is much smaller than the light wavelength. As shown in Figure 3a, a theoretical simulation of the absorption spectrum in possession of remarkable near-infrared absorption band in accord with the experimental spectrum is obtained by the Mie–Gans theory[8,31] which is used to describe LSPRs in nanocrystals (see the Supporting Information). As eq 1 indicated, the LSPR frequency in the near-infrared band is sensitive to the dielectric constant of the surrounding medium ε_m (or the refractive index). The peak of LSPR absorption red-shifts as the refractive index of the surrounding solvent increases (Figure S3, Supporting Information), which further indicates that the near-infrared absorption band originates from LSPRs.[6,8,9]

When we increased the surface-treatment cycles with the same oxygen exposure time mentioned above, the corresponding LSPR absorption peak blue-shifted from ~1260 nm (curve 1 in Figure 3b) to ~1130 nm (curve 4 in Figure 3b). It is noticeable that a blue-shift effect of LSPRs in Figure 3b does not originate from the change of the dielectric constant of the surrounding medium because the refractive index of TCE (1.51) is larger than that of OYA (1.458) detached during the surface-treatment cycles. Figure 4 illustrates an obvious blue-

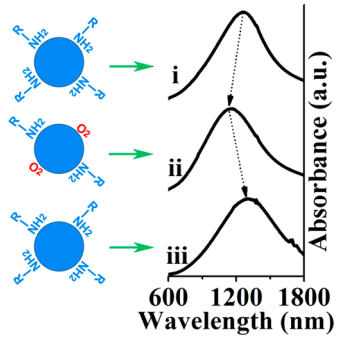

Figure 4. Schematic illustration of the process of LSPR shifts. LSPR blue-shift (curve i to ii) when OYA is unloaded and oxygen is adsorbed on the surface of CuS nanodisk. LSPRs revert (curve ii to iii) when CuS nanodisk is repassivated by OYA.

shift of the LSPR wavelength after exposure to air, compared with its original spectrum measured immediately after synthesis under oxygen-free atmosphere (curve i to ii). However, this blue-shift is revertible by repassivation of OYA, as demonstrated in Figure 4 (curve ii to iii). In fact, previous studies on generating and removing LSPRs in Cu_2S and Cu_2Se nanocrystals by oxidation and reduction always referred to phase transition to non-stoichiometric structures and significant effect on the interband transition.[10,11] In our cases, no distinct change was detected on the interband transition absorption during surface-treatment processes because no morphology or crystal structure transition happened as checked by TEM and XRD. However, accompanied with the corresponding blue-shift and reversion of LSPRs, the ratio of O/Cu increases and decreases, respectively, as shown in Table 1 derived from XPS (Figure S5, Supporting Information).

The blue-shift of LSPRs exhibits a gradually decreased rate with time and reached saturation after several days in air. Less blue-shift in LSPR wavelength is observed for CuS nanodisk dispersion stored in a glovebox filled by nitrogen with 100 ppm

Table 1. The Relative Variation of Integrated Areas of O and Cu 2p3/2 in XPS Spectra

area ratio	before exposure	oxygen exposure	repassivation
O/Cu	0.15	0.27	0.14

dx.doi.org/10.1021/am4039568 | ACS Appl. Mater. Interfaces 2013, 5, 10473–10477

oxygen, compared with that stored under ambient conditions (Figure 5a). According to eqs 1 and 2, the LSPR frequency is

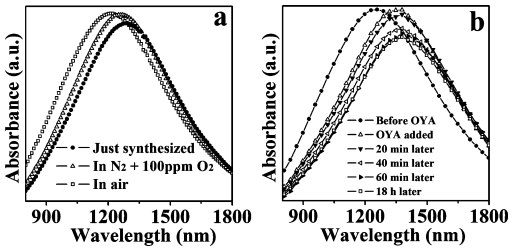

Figure 5. (a) The absorption spectra of CuS nanodisk dispersion stored in air and in a glovebox filled by nitrogen with 100 ppm oxygen in contrast to their original one measured just after synthesis. (b) The temporal variation of absorption spectra of CuS nonodisks after being repassivated by OYA.

tunable by varying the carrier density. The adsorbed oxygen acts as an electron acceptor on the surface of CuS nanodisks, and is deduced to enhance the hole density via withdrawing electrons from the nanocrystals. This enhancement results in the blue-shift of LSPRs, which is similar to how oxygen adsorption increased the conductivity[32] of the p-type oxide semiconductor. We thought that the oxygen can be adsorbed due to molecular electrostatic adhesion, and be removed, which allows LSPRs to blue-shift and revert by surface unloading and reloading OYA ligand (not reducing agent). Surface OYA ligand coordinating to CuS through nitrogen atom hardly withdraws an electron but would share its lone pair with the coordinated nanodisk.[33] Therefore, the blue-shift of LSPRs reverts when the enhanced hole density is diminished by OYA repassivating to desorb oxygen on the surface of CuS nanodisks. The reverting of LSPRs was detectable by spectroscopy immediately after the repassivation process. A bit larger red-shift was observed in the following tens of minutes (Figure 5b), implying nearly complete passivation on the surface of CuS nanodisks. The evolution was nearly completed within 60 min after the adding of OYA.

We therefore thought the surface-treatment cycles unloaded OYA from CuS nanocrystals for a decreased resistance of oxygen adsorption. OYA serves as a block for preventing oxygen adsorption on the surface of CuS nanodisks. The surface coverage of OYA on CuS nanodisks decreases for more surface-treatment cycles, which results in a larger blue-shift of LSPRs due to more oxygen being adsorbed. However, more than eight surface-treatment cycles will make it unable to reverse the shift of LSPRs. A possible chemical adsorption might occur and be responsible for this irreversibility, once a large dose of oxygen has been adsorbed by CuS nanodisks with higher ligand coverage exposed to air for a longer time or the ones with much lower ligand coverage.[10−12]

Figure 6 further displays how different surface ligands (i.e., OYA, OA, and DDT) affect the absorption spectra of CuS nanodisks. Compared with the LSPRs of CuS nanodisks with OYA ligand, the LSPRs blue-shift after OYA was exchanged to OA, while they red-shift for DDT ligand. The effect of media dielectric constant on LSPRs may be ruled out because the refractive indices of these ligands are nearly the same (∼1.458). However, their electron-withdrawing abilities are different, which are responsible for the shift of LSPRs. OA is usually referred to as a Lewis acid which is able to accept electrons. Both OYA and DDT are Lewis bases which are able to denote

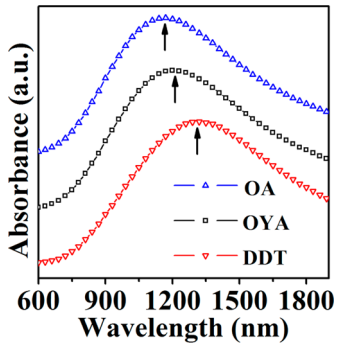

Figure 6. The absorption spectra of CuS nanodisks with different ligands by exchanging ligands on the surface of nanodisks.

electrons, and the electron-denoting ability of OYA is weaker than that of DDT.[34] Therefore, OA increases the hole density of CuS nanodisks, resulting in the blue-shift of LSPRs when we used OA to replace OYA. In constrast to OA, DDT can denote more electrons on the surface than OYA, and then decrease the hole density in CuS nanodisks, which leads to LSPR red-shift in the case of DDT replacing OYA. All of these results further indicate that the electron-withdrawing abilities of surface adsorbed species play a key role in tuning LSPRs in CuS nanodisks.

4. SUMMARY

We demonstrate the revertible shift of LSPRs resulting from oxygen exposure and ligand repassivation on CuS nanodisks. The LSPR absorption in the near-infrared region is sensitive to the oxygen adsorption and desorption when the surface ligands on CuS nanodisks are unloaded and reloaded. The withdrawing and restoring processes of electrons on the surface are an essential physical mechanism behind this revertible shift generated in covellite CuS nanodisks. All of these have been confirmed by LSPRs tuned through the oxygen exposure dose and time, and the surface ligand coverage and exchange. These routes may provide more opportunities and new perspectives for semiconductor nanocrystals with tunable LSPRs in optical applications.

■ ASSOCIATED CONTENT

Ⓢ Supporting Information

TGA curve of copper ethylxanthate, HRTEM of single CuS nanodisk, solvent refractive index dependence of absorption spectra, FTIR spectra, XPS spectra, and theoretical simulation of LSPR absorption spectrum. This material is available free of charge via the Internet at http://pubs.acs.org.

■ AUTHOR INFORMATION

Corresponding Authors

*E-mail: xinchen@mail.sitp.ac.cn (X.C.).
*E-mail: ndai@mail.sitp.ac.cn (N.D.).

Notes

The authors declare no competing financial interest.

■ ACKNOWLEDGMENTS

This work was funded by National Basic Research Program of China (2012CB934301 and 2011CBA00905), NSFC (61376016 and 61290304), CAS (KSZD-EW-Z-018), and STCMS.

REFERENCES

(1) Hutter, E.; Fendler, J. H. *Adv. Mater.* **2004**, *16*, 1685−1706.
(2) Jain, P. K.; Huang, X. H.; El-Sayed, I. H.; El-Sayed, M. A. *Acc. Chem. Res.* **2008**, *41*, 1578−1586.
(3) Moreau, A.; Ciraci, C.; Mock, J. J.; Hill, R. T.; Wang, Q.; Wiley, B. J.; Chilkoti, A.; Smith, D. R. *Nature* **2012**, *492*, 86−89.
(4) Mulvaney, P. *Langmuir* **1996**, *12*, 788−800.
(5) Kanehara, M.; Koike, H.; Yoshinaga, T.; Teranishi, T. *J. Am. Chem. Soc.* **2009**, *131*, 17736−17737.
(6) Luther, J. M.; Jain, P. K.; Ewers, T.; Alivisatos, A. P. *Nat. Mater.* **2011**, *10*, 361−366.
(7) Buonsanti, R.; Llordes, A.; Aloni, S.; Helms, B. A.; Milliron, D. J. *Nano Lett.* **2011**, *11*, 4706−4710.
(8) Manthiram, K.; Alivisatos, A. P. *J. Am. Chem. Soc.* **2012**, *134*, 3995−3998.
(9) Niezgoda, J. S.; Harrison, M. A.; McBride, J. R.; Rosenthal, S. J. *Chem. Mater.* **2012**, *24*, 3294−3298.
(10) Dorfs, D.; Härtling, T.; Miszta, K.; Bigall, N. C.; Kim, M. R.; Genovese, A.; Falqui, A.; Povia, M.; Manna, L. *J. Am. Chem. Soc.* **2011**, *133*, 11175−11180.
(11) Kriegel, I.; Jiang, C. Y.; Rodriguez-Fernandez, J.; Schaller, R. D.; Talapin, D. V.; da Como, E.; Feldmann, J. *J. Am. Chem. Soc.* **2012**, *134*, 1583−1590.
(12) Silvester, E. J.; Grieser, F.; Sexton, B. A.; Healy, T. W. *Langmuir* **1991**, *7*, 2917−2922.
(13) Artemyev, M. V.; Gurin, V. S.; Yumashev, K. V.; Prokoshin, P. V.; Maljarevich, A. M. *J. Appl. Phys.* **1996**, *80*, 7028−7035.
(14) Zhang, P.; Gao, L. *J. Mater. Chem.* **2003**, *13*, 2007−2010.
(15) Zhang, H. T.; Wu, G.; Chen, X. H. *Mater. Chem. Phys.* **2006**, *98*, 298−303.
(16) Nozaki, H.; Shibata, K.; Ohhashi, N. *J. Solid State Chem.* **1991**, *91*, 306−311.
(17) Hsu, S. W.; On, K.; Tao, A. R. *J. Am. Chem. Soc.* **2011**, *133*, 19072−19075.
(18) Hsu, S. W.; Bryks, W.; Tao, A. R. *Chem. Mater.* **2012**, *24*, 3765−3771.
(19) Kanehara, M.; Arakawa, H.; Honda, T.; Saruyama, M.; Teranishi, T. *Chem.—Eur. J.* **2012**, *18*, 9230−9238.
(20) Zhao, Y.; Pan, H.; Lou, Y.; Qiu, X.; Zhu, J.; Burda, C. *J. Am. Chem. Soc.* **2009**, *131*, 4253−4261.
(21) Liu, Y. F.; Ge, M. Y.; Yue, Y.; Sun, Y.; Wu, Y. Z.; Chen, X.; Dai, N. *Phys. Status Solidi RRL* **2011**, *5*, 113−115.
(22) Xie, Y.; Carbone, L; Nobile, C.; Grillo, V.; D'Agostino, S.; Della Sala, F.; Giannini, C.; Altamura, D.; Oelsner, C.; Kryschi, C.; Cozzoli, P. D. *ACS Nano* **2013**, *7*, 7352−7369.
(23) Zhuang, Z.; Peng, Q.; Zhang, B.; Li, Y. *J. Am. Chem. Soc.* **2008**, *130*, 10482−10483.
(24) Lim, W. P.; Wong, C. T.; Ang, S. L.; Low, H. Y.; Chin, W. S. *Chem. Mater.* **2006**, *18*, 6170−6177.
(25) Tang, A. W.; Qu, S. C.; Li, K.; Hou, Y. B.; Teng, F.; Cao, J.; Wang, Y. S.; Wang, Z. G. *Nanotechnology* **2010**, *21*, 285602.
(26) Grozdanov, I.; Najdoski, M. *J. Solid State Chem.* **1995**, *114*, 469−475.
(27) Gotsis, H. J.; Barnes, A. C.; Strange, P. *J. Phys.: Condens. Matter* **1992**, *4*, 10461−10468.
(28) Liang, W.; Whangbo, M. H. *Solid State Commun.* **1993**, *85*, 405−408.
(29) Saito, S.; Kishi, H.; Nié, K.; Nakamaru, H.; Wagatsuma, F.; Shinohara, T. *Phys. Rev. B* **1997**, *55*, 14527−14535.
(30) Parreira, P.; Lavareda, G.; Amaral, A.; Botelho do Rego, A. M.; Conde, O.; Valente, J.; Nunes, F.; Nunes de Carvalho, C. *J. Alloys Compd.* **2011**, *509*, 5099−5104.
(31) Maier, S. A. *Plasmonics: Fundamentals and Applications*; Springer: New York, 2007; pp 66−72.
(32) Wang, C.; Fu, X. Q.; Xue, X. Y.; Wang, Y. G.; Wang, T. H. *Nanotechnology* **2007**, *18*, 145506.
(33) Trinh, T. T.; Ozaki, T.; Maenosono, S. *Phys. Rev. B* **2011**, *83*, 104413.
(34) Green, M. *J. Mater. Chem.* **2010**, *20*, 5797−5809.